Electronic Supplementary Information

Monomer-Assembly Template-Directed Synthesis of Conjugated Porous Polymer Microtubular Bundles

Wenbei Zhang,[a] Tianlu Cui,[b] Shuai Bi,[a] Lie Ma,[a] Deng Lu,[a] Dongqing Wu[a] and Fan Zhang*[a]*

[a]School of Chemistry and Chemical Engineering, State Key Laboratory of Metal Matrix Composites, Shanghai Jiao Tong University, Shanghai 200240, P. R. China
[b]Department of Material and Chemical Engineering, Zhengzhou University of Light Industry, Zhengzhou 450002, P. R. China.
E-mail: wudongqing@sjtu.edu.cn; fan-zhang@sjtu.edu.cn

Contents

1. Methods

Materials

3,4,9,10-Perylenetetracarboxylic dianhydride, 4-formylphenylboronic acid was purchased from Sigma. Benzohydrazide were purchased from Aladdin (Shanghai, China). Ethanol, toluene, dichloromethane, tetrahydrofuran (THF), DMAc, and all the other solvents were purchased from Adamas Reagent. All the chemicals were of analytical grade and used as received without further purification.

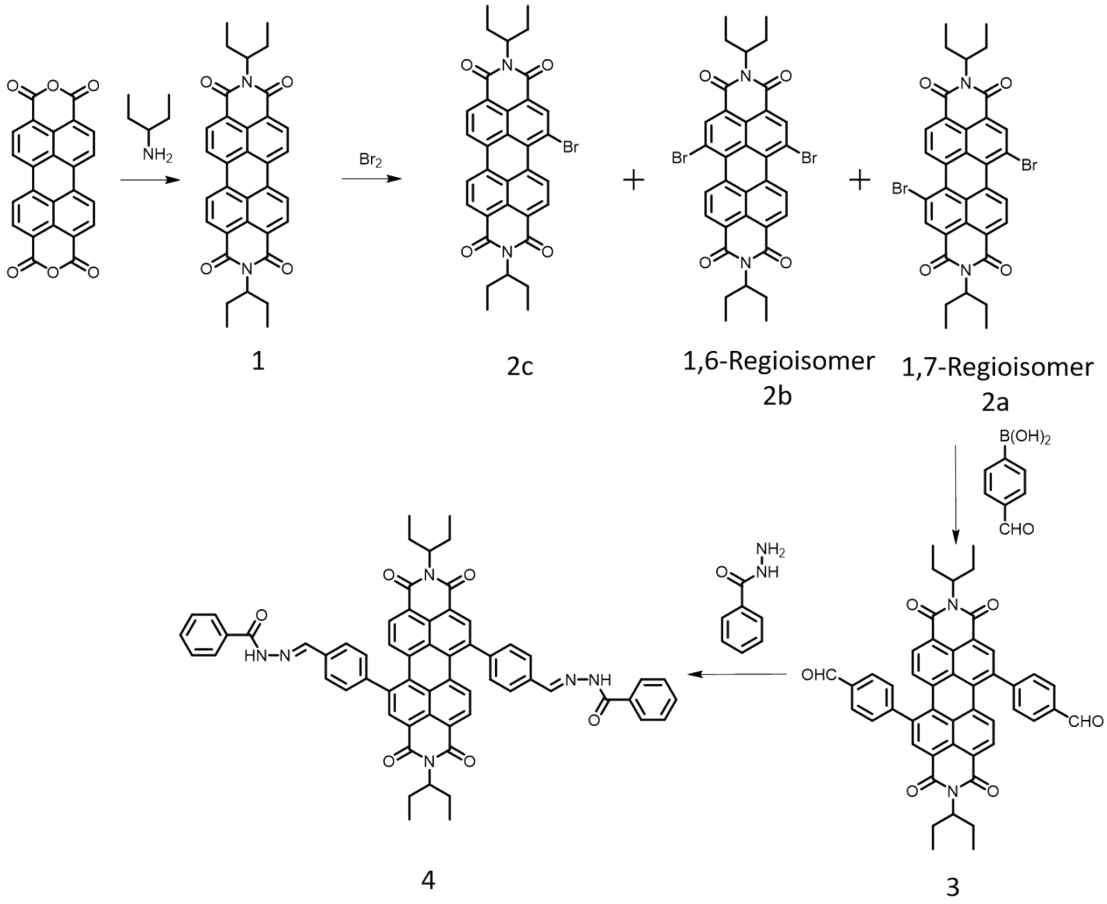

Scheme S1. Synthesis route of *N,N*-bis(1-ethylpropyl)-1,7-bis(4-formyl-phenyl)-perylene- 3,4,9,10-tetracarboxydiimide and reference compound.

Bromination of *N,N*-bis(ethylpropyl)-perylene-3,4,9,10-tetracarboxylic Diimide.[1]

N,N-bis(ethylpropyl)perylene-3,4,9,10-tetracarboxylic bisimide (1) was prepared from 3,4,9,10-perylenetetracarboxylic dianhydride using a reported procedure.[1] Typically, the mixture of 1-ethylpropylamin (1.3 g, 15 mmol) and 3,4,9,10-perylenetetracarboxylic dianhydride (980 mg, 2.5 mmol) in imidazole (15 g) was heated at 140 °C for 6 h. Before complete cooling to room temperature, the mixture was diluted with ethanol (50 mL) and hydrochloric acid (100 mL, 2 M) to remove the crystallized imidazole and then stirred for 1 h. Subsequently, the precipitate in the mixed solution was collected by vacuum filtration, washed with distilled water, and dried at 120 °C overnight to yield compound 1 (1.2 g, yield ~ 90 %). ^{1}H NMR (400 MHz, $CDCl_3$, ppm): 0.93 (t, 12H), 1.94 (m, 4H), 2.27 (m, 4H), 5.07 (m, 2H), 8.61–8.69 (m, 8 H, ArH). ^{13}C NMR (100 MHz, $CDCl_3$, ppm): 11.4, 25.0, 57.4, 123.0, 123.5, 126.4, 129.6, 131.4, 134.5, 164.1.

In the bromination process, the mixture of 1 (2 g, 3.77 mmol) and bromine (31.1 g, 0.194 mol) in dichloromethane (100 mL) was stirred at 25 °C in a round-bottom flask for 2 days. The excess of bromine was removed by air bubbling, and the solvent was removed under vacuum. The crude product was purified by column chromatography with silica gel as stationary phase and chloroform as eluent. The first band was collected to afford dibromoperylene diimide (red solid, 1.95 g, yield ~ 75%) as the mixture of regioisomers (2a : 2b = 5:1). The second band yielded bromo-*N,N*-bis(ethylpropyl)-perylene-3,4,9,10-tetracarboxylic diimide (2c, 230 mg, 10%). ^{1}H NMR (400 MHz, $CDCl_3$, ppm): 9.75 (d, 1H), 8.90 (s, 1H), 8.67 (m, 3H), 8.59 (d, 1H), 8.57 (d, 1H), 5.05 (m, 2H), 2.25 (m, 4H), 1.92 (m, 4H), 0.92 (m, 12H). ^{13}C NMR (100 MHz, $CDCl_3$, ppm):

164.1, 163.8, 163.7, 162.9, 139.0, 133.9, 133.6, 133.5, 130.9, 130.4, 129.0, 128.8, 128.2, 128.0, 127.1, 124.0, 123.9, 123.5, 123.2, 122.8, 120.8, 58.1, 57.9, 25.0, 24.9, 11.1, 11.0.

The regio-isomeric dibromoperylene diimides 2a and 2b could be separated by recrystallization. The mixture (200 mg) of 2a and 2b was crystallized from 50 mL of CH_2Cl_2: hexane (v/v, 1:1) at room temperature for 5 days. The crystallization was repeated at the same conditions for two more times to yield of pure 1,7-dibromo-*N,N*-bis(ethylpropyl)perylene-3,4,9,10-tetracarboxylic diimide (2a, 120 mg, yield ~60%) as a red solid. ^{1}H NMR (400 MHz, $CDCl_3$, ppm): 9.50 (d, 2H), 8.91 (s, 2H), 8.70 (d, 2H), 5.05 (m, 2H), 2.25 (m, 4H), 1.95 (m, 4H), 0.93 (t, 12H). ^{13}C NMR (100 MHz, $CDCl_3$, ppm): 163.7, 163.1, 138.3, 138.0, 133.0, 132.8, 130.2, 129.9, 129.5, 128.6, 128.5, 127.4, 123.7, 123.3, 120.8, 58.2, 25.2, 11.3, 11.2.

Synthesis of *N,N*-bis(1-ethylpropyl)-1,7-bis(4-formyl-phenyl)-perylene-3,4,9,10-tetracarboxydiimide (bPDI)

Compound 2a (1032 mg, 1.5 mmol) and 4-formylphenylboronic acid (900 mg, 6 mmol) were firstly added to a schlenk flask with toluene (20 ml), ethanol (6 ml) and K_2CO_3 aqueous solution (6 ml, 3.5 mol L^{-1}) under nitrogen flow. After further degassing for 30 min, $Pd(PPh_3)_4$ (173.3 mg, 0.15 mmol) was added to the mixture, which was then stirred at 80 °C overnight. Subsequently, the mixture was poured into brine and extracted by dichloromethane for several times. The organic phase was dried over Mg_2SO_4 and the solvent was evaporated in vacuum. The crude product was purified by column chromatography with silica gel as stationary phase and CH_2Cl_2 as

the eluent to give **bPDI** as red powder (653 mg, yield ~59%). ^{1}H NMR (400 MHz, $CDCl_3$, ppm): 0.89 [t, 12H, N-CH(CH_2CH_3)$_2$], 1.90 [m, 4H, N-CH(CH_2CH_3)$_2$], 2.23 [m, 4H, N-CH(CH_2CH_3)$_2$], 5.03 [m, 2H, N-CH(CH_2CH_3)$_2$], 7.76 (dd, 6H, ArH), 8.03 (d, 4H, ArH), 8.14 (d, 2H, ArH), 8.62 (s, 2H, ArH), 10.14 (s, 2H, CHO). ^{13}C NMR (100 MHz, $CDCl_3$, ppm): 11.3, 25.0, 57.8, 114.1, 122.6, 128.2, 129.1, 130.0, 130.7, 131.4, 132.5, 134.2, 134.9, 136.1, 139.7, 148.2, 191.4. ESI-MS mass spectrum: m/z calcd. for $C_{48}H_{39}N_2O_6$ 739.2808; HR-ESI observed 739.2814.

Synthesis of the reference compound

Following the method towards the porous polymer, a reference compound was synthesized using benzohydrazide (13.6 mg, 0.1 mmol) and **bPDI** (31.7 mg, 0.05 mmol) as starting materials. The mixture was sonicated for 1 min, degassed *via* three freeze–pump–thaw cycles, sealed under vacuum, and kept at 120 °C for 1 days. Then, the mixture was poured into brine and extracted by dichloromethane for several times. The organic phase was dried over Mg_2SO_4 and the solvent was evaporated in vacuum. The crude product was purified by column chromatography with silica gel as stationary phase and CH_2Cl_2 as the eluent to give modeling compound as red powder (37.8 mg, 85%). ESI-MS mass spectrum: m/z calcd. for $C_{62}H_{50}N_6O_6$ 974.3792; HR-ESI observed 974.3881.

Synthesis of PDI polymer at para-position (control sample)

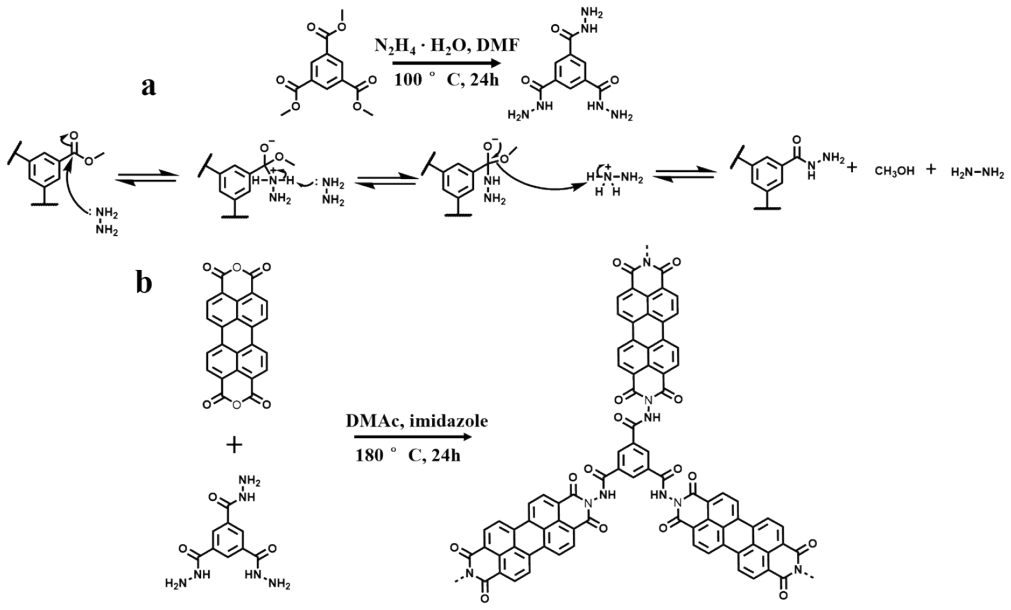

Scheme S2. (a) Synthesis scheme and mechanism of TPH, (b) Synthesis route of the control sample.

Perylene dianhydride (35.3 mg, 0.09 mmol) was taken in imidazole (5 g) and stirred at 150 °C under N_2 atmosphere until it dissolves. a solution of 1,3,5-benzene-tricarbohydrazide[2] (15mg, 0.06 mmol) in DMAc (5 mL) was added dropwise and stirred at 180 °C for 24 h[3]. After this the reaction mixture was cooled to 100 °C and methanol was added (20 mL). The precipitate formed was collected by filtration followed washing with DMF (20 mL) and methanol (20 mL). This solid precipitate was dried overnight at 120 °C under vacuum to yield control sample as a dark red solid (40 mg, yield ~ 81 %). Elemental analysis (%) $(C_{30}H_{12}N_4O_6)n$ theoretical C (68.71), H (2.31), N (10.68), O (18.3); found C (70.72), H (5.52), N (10.59), O (12.94).

General polymerization procedure.

All polymerization reactions were carried out in sealed pyrex tube. For all polymers, DMAc was used as solvent. The molar ratio of **TPH** to the corresponding aldehyde was set to 2:3 to provide equimolar amounts of amine and aldehyde groups.

Synthesis of bPDI-AHD-TPH at different time intervals.

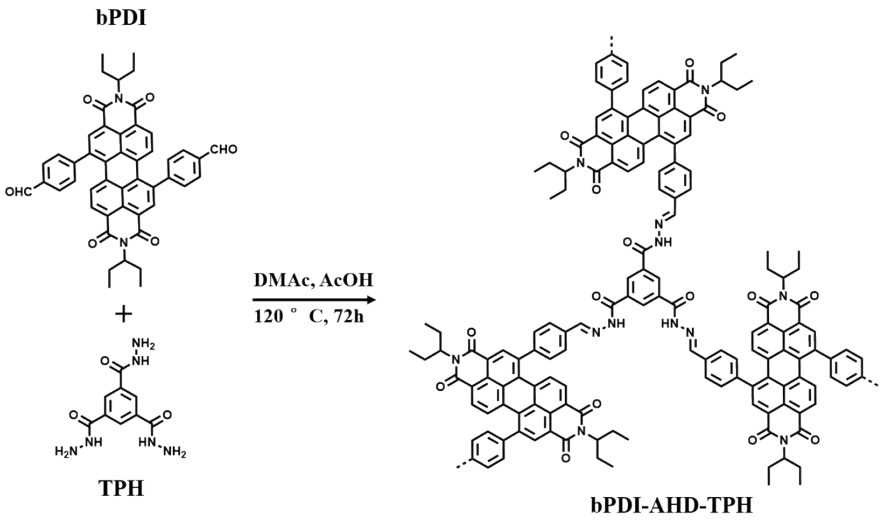

Scheme S3. Synthesis route of **bPDI-AHD-TPH.**

The reaction mixture was distributed to several pyrex tubes and individual samples were removed from the oven after specified time intervals (1, 12 and 24 h). After cooling to room temperature, precipitates were collected and dried in a similar fashion as described before.

Synthesis of Ph-AHD-TPH and BiPh-AHD-TPH

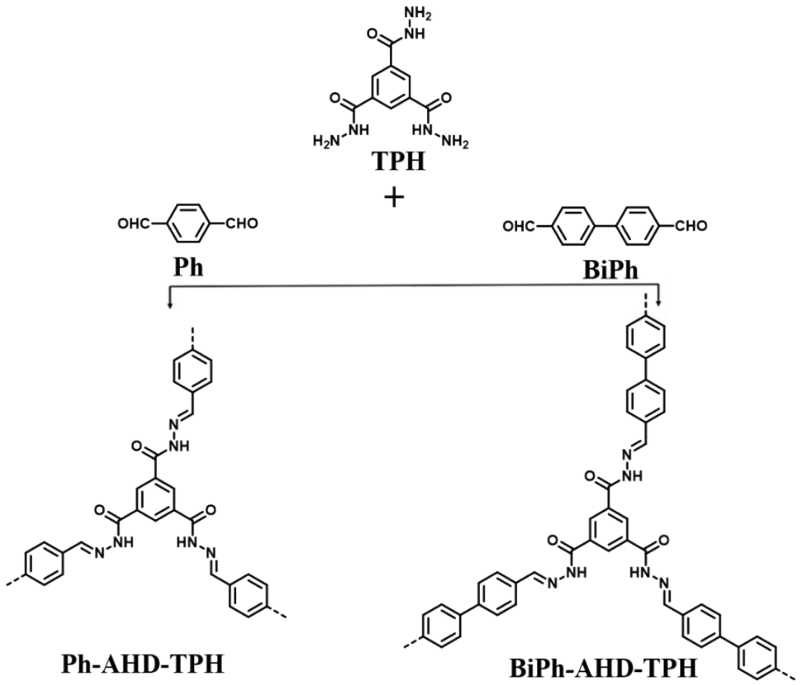

Scheme S4. Synthesis route of **Ph-AHD-TPH** and **BiPh-AHD-TPH**.

The mixture of terephthalaldehyde (**Ph**, 16 mg, 0.12 mmol) or 4,4-biphenyldicarboxaldehyde (**BiPh**, 25 mg, 0.12 mmol), **TPH** (20mg, 0.08 mmol), acetic acid (0.2 mL, 6M) and DMAc (2 mL) were added in a pyrex tube. The mixture was sonicated for 1 min, degassed *via* three freeze–pump–thaw cycles, sealed under vacuum, and kept at 120 °C for 3 days. After cooled to room temperature, the precipitate in the mixture was collected by centrifugation, washed with DMAc and CH_2Cl_2, soaked in THF for 3 hours, and dried at 120 °C overnight, to yield **Ph-AHD-TPH** and **BiPh-AHD-TPH** as white solids (yield: ~ 80 %).

Structural characterization

Scanning electron microscopy (SEM) was performed using an FEI Sirion-200 (FEI Co., USA) field emission scanning electron microscope. Transmission electron microscopy (TEM) observations were carried out with a JEOL-2100 (JEOL Ltd., Japan) electron microscope at an operating voltage of 200 kV. The samples were firstly dispersed in alcohol, and the suspensions were dropped onto a copper grid covered with lacey support films. X-ray diffraction (XRD) measurements were performed using a Rigaku D/Max 2500 X-ray di□ractometer with Cu Kα radiation (k=1.54 Å) at a generator voltage of 40 kV and a generator current of 50 mA with a scanning speed of 5° min^{-1} from 5° to 60°. The nitrogen adsorption/desorption isotherms were measured *via* an Autosorb-iQA3200-4 sorption analyzer (Quantatech Co., USA). Before measurement, the samples were degassed in vacuum at 120 °C for more than 10 h. Solid-state ^{13}C NMR analysis was conducted on a Bruker AVANCE III 300

Spectrometer. Samples were spun at 5 kHz in a 4 mm zirconium rotor within a magic-angle spinning (MAS) probe. An acquisition time of 20 ms, a contact time of 1 ms, and a 6.5 μs pre-scan delay were used. The recycle time was 2 s in order to obtain fully relaxed spectra.

2. NMR spectra and MS of monomers

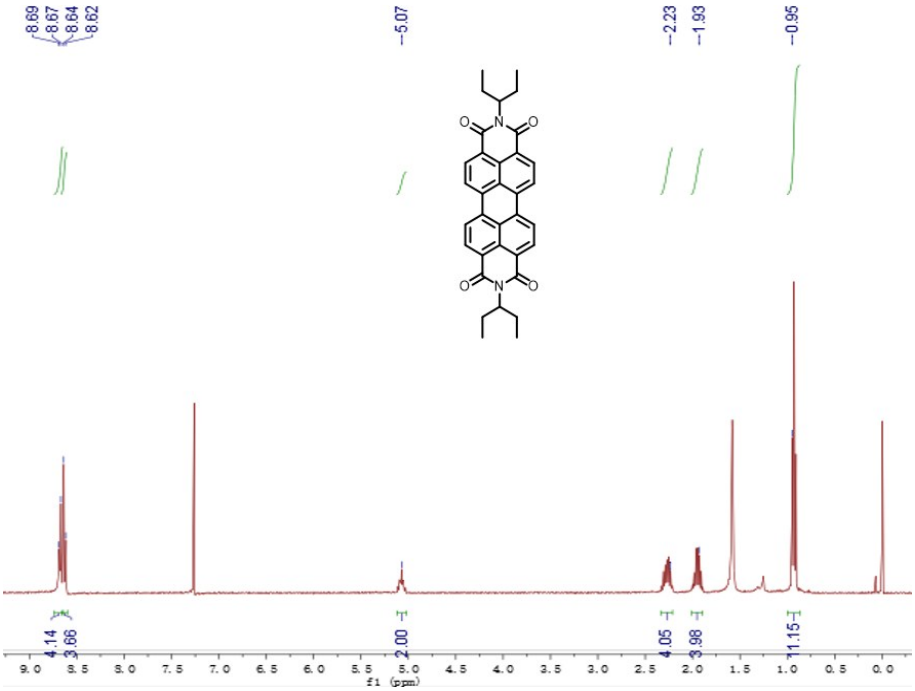

Figure S1. ^{1}H NMR spectrum of monomer 1.

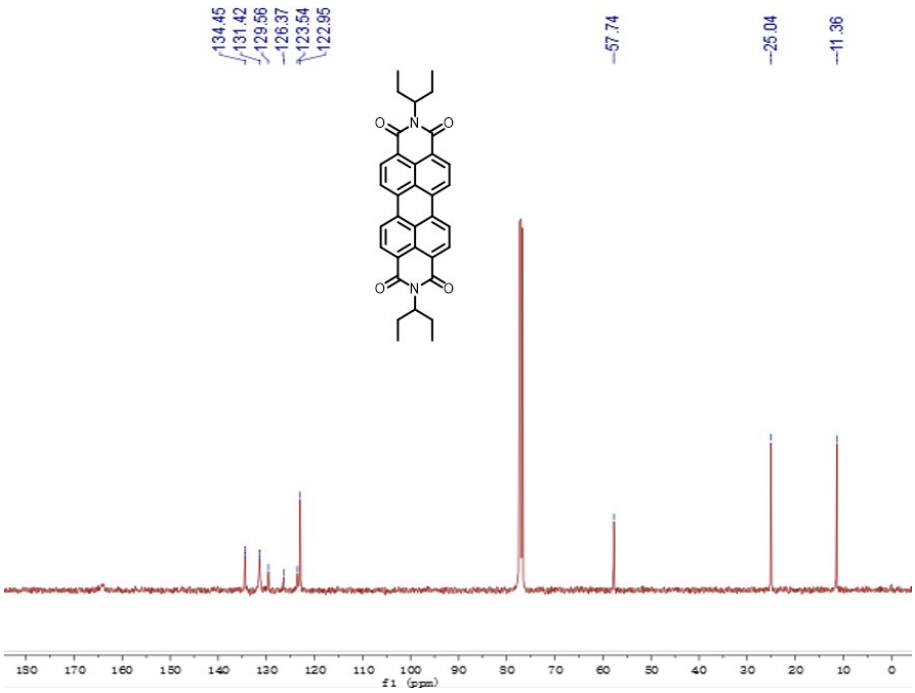

Figure S2. ^{13}C NMR spectrum of monomer 1.

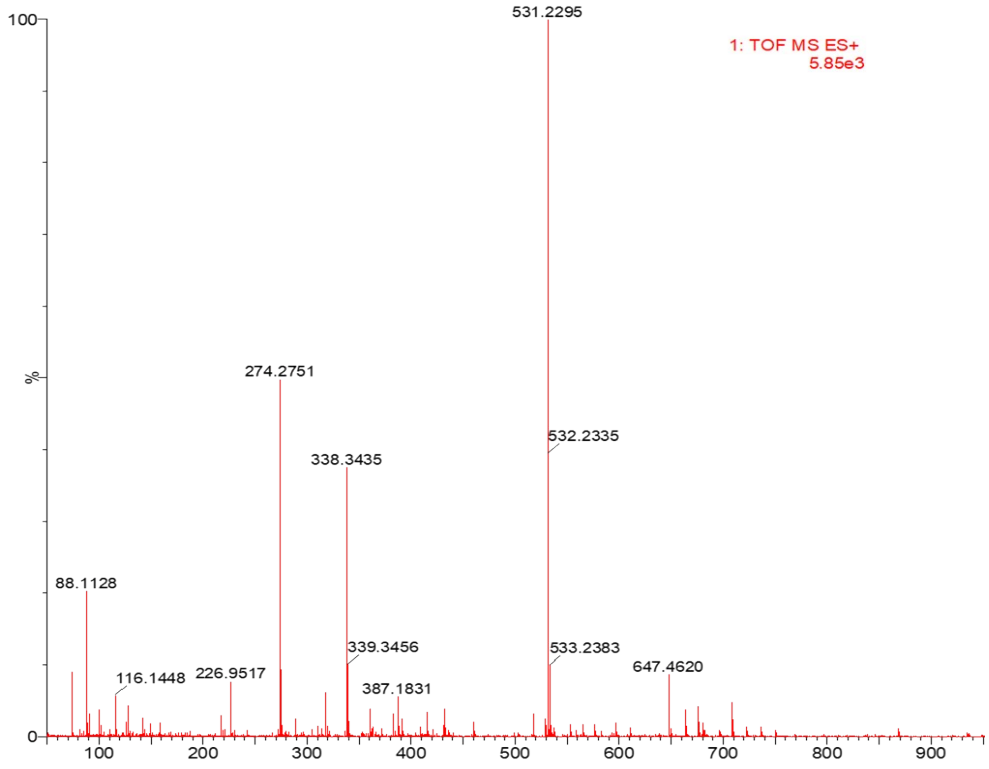

Figure S3. Mass spectrum of monomer 1.

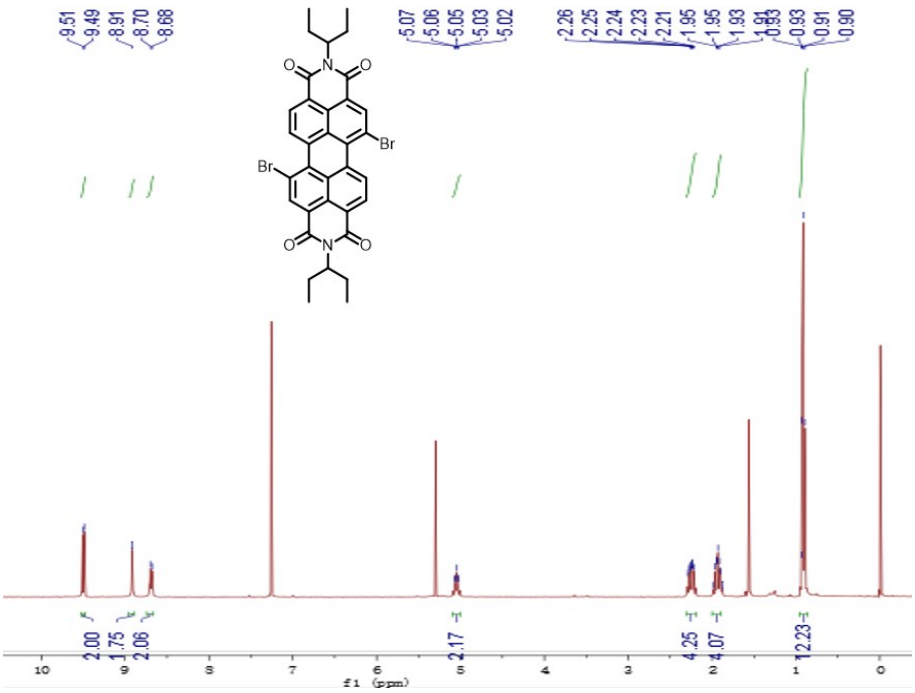

Figure S4. ^{1}H NMR spectrum of monomer 2a.

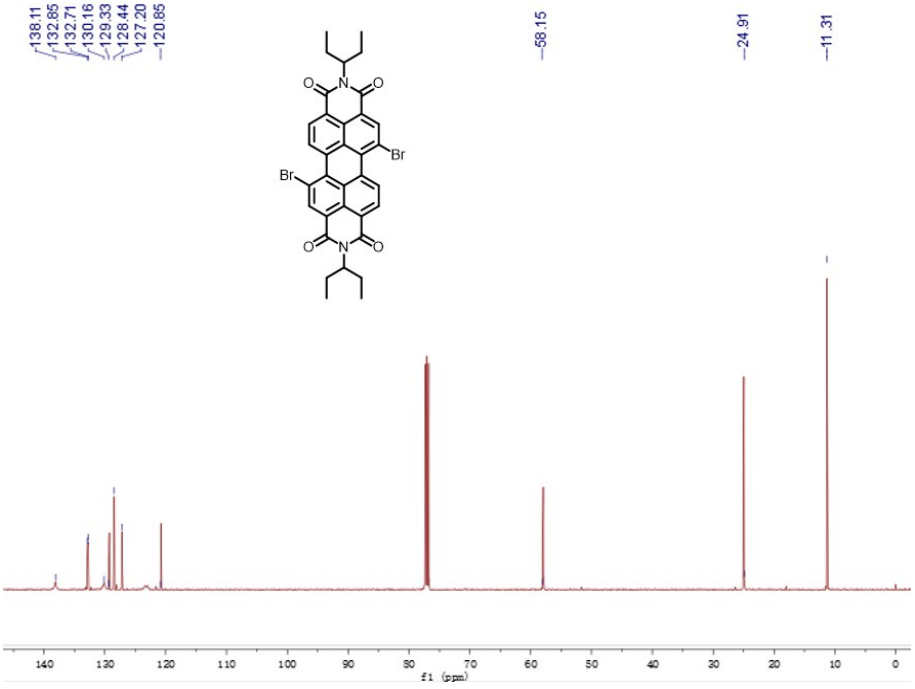

Figure S5. ^{13}C NMR spectrum of monomer 2a.

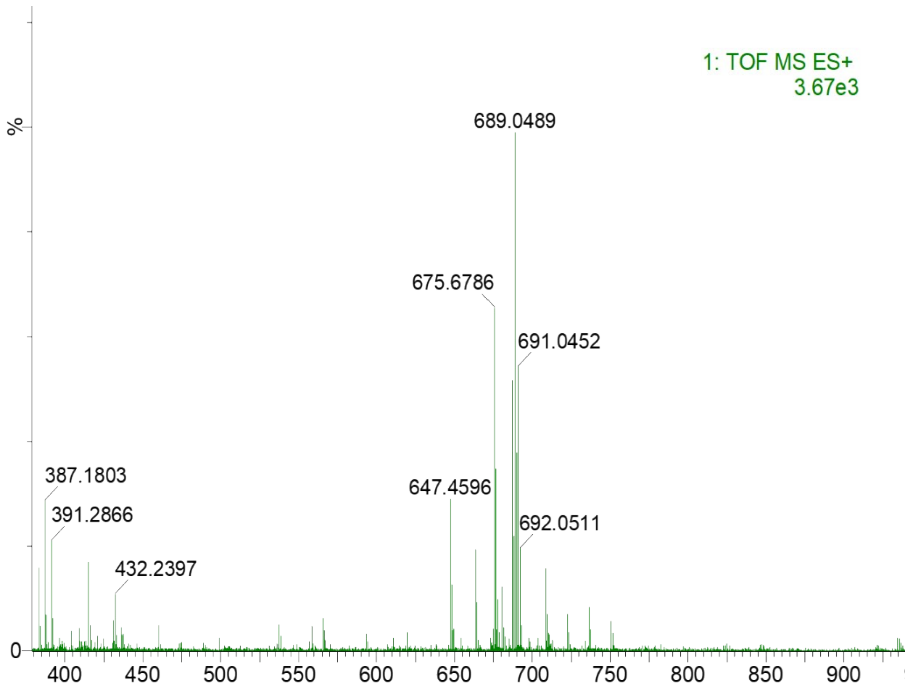

Figure S6. Mass spectrum of monomer 2a

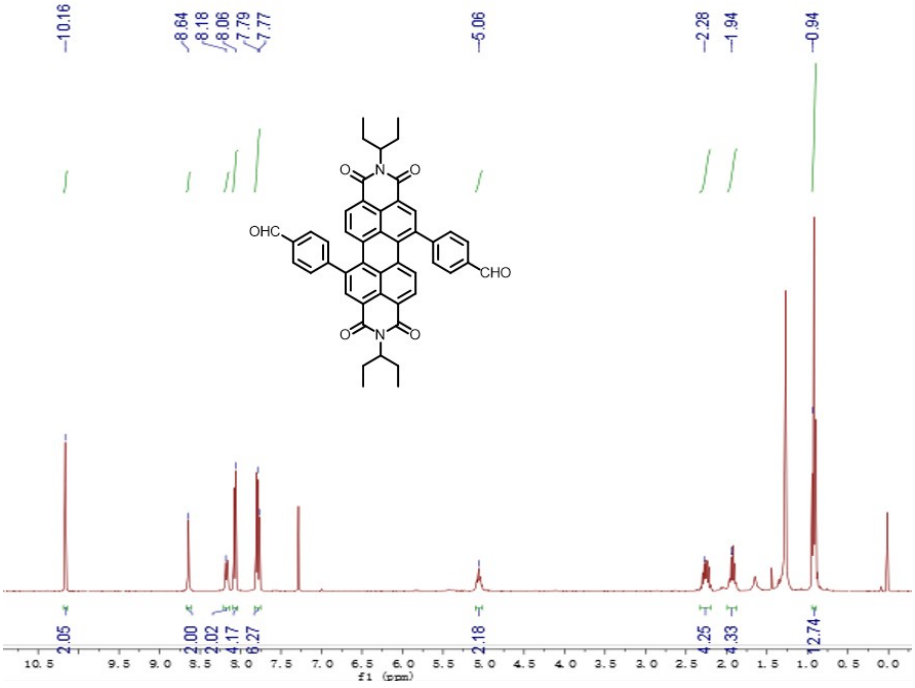

Figure S7. ^{1}H NMR spectrum of **bPDI**.

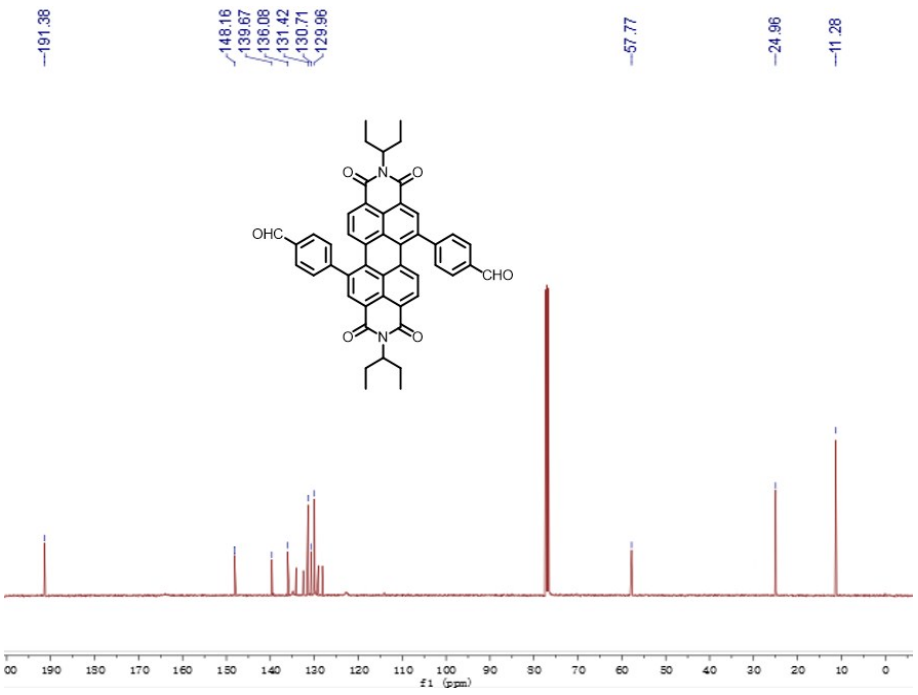

Figure S8. ^{13}C NMR spectrum of **bPDI**.

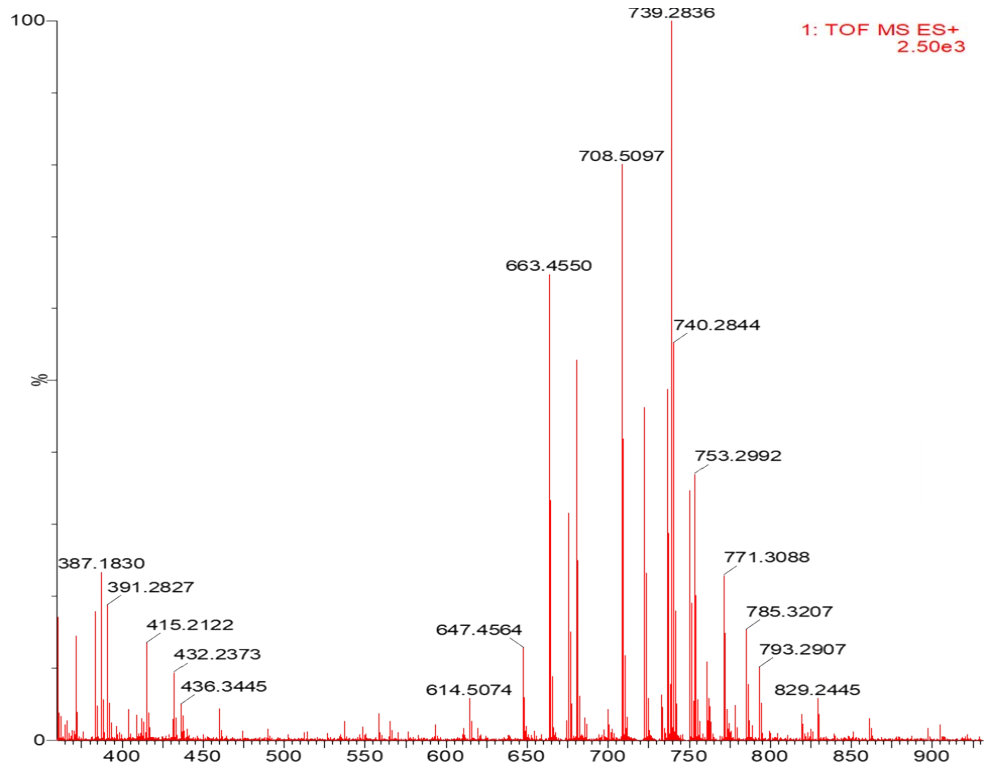

Figure S9. Mass spectrum of **bPDI**.

3. Supplementary figures

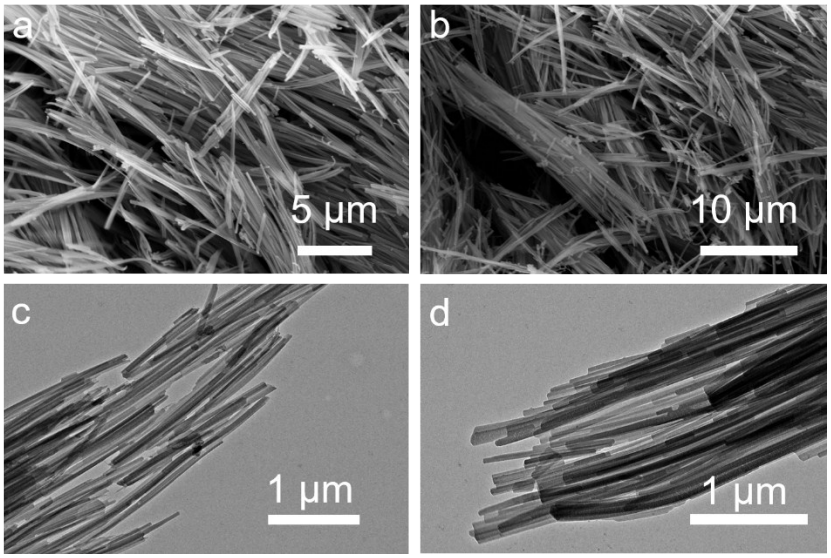

Figure S10. SEM and TEM images of **TPH**.

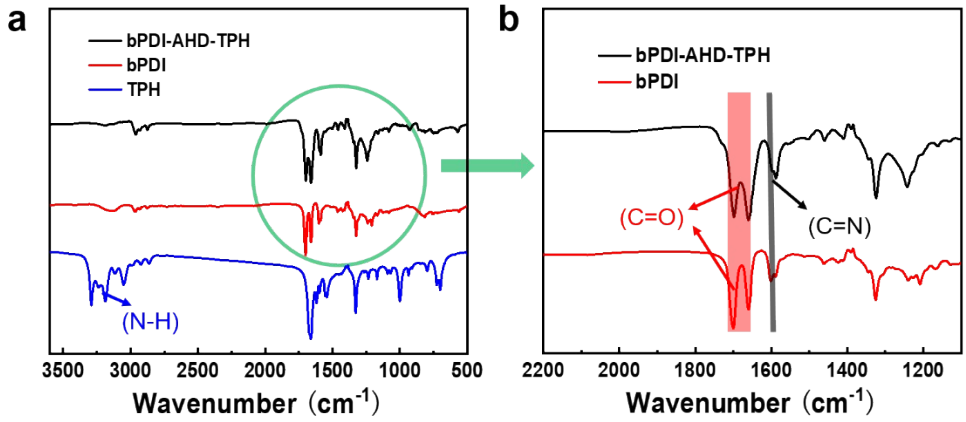

Figure S11. FT-IR spectra of **bPDI-AHD-TPH** and monomers.

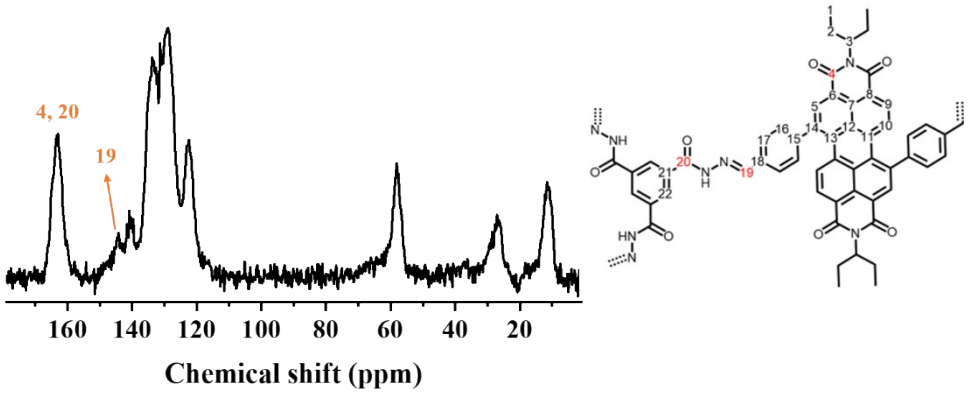

Figure S12. Solid-state ^{13}C CP/MAS NMR spectrum of **bPDI-AHD-TPH**.

Table S1. Peak assignments for solid-state ^{13}C CP/MAS NMR spectrum of **bPDI-AHD-TPH**.

Signal (ppm)	Assignment	Comment
11	1	Methyl carbon
25	2	Methylene carbon
58	3	tertiary carbon
123	7,12	perylene ring carbons
130-134	5,6,8,9,10,11,13,16,17,21, 22	perylene ring and Aromatic C-H carbons carbon
141	14,15,18	Aromatic quaternary carbon
144	19	Imine carbon
163	4,20	Amide and imide carbon

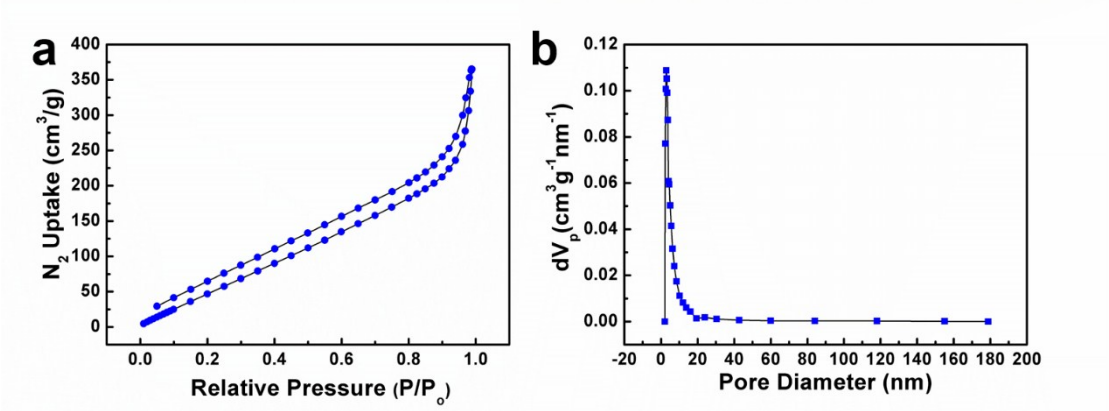

Figure S13. Nitrogen adsorption/desorption isotherms (a) and pore distribution (b) of **bPDI-AHD-TPH**.

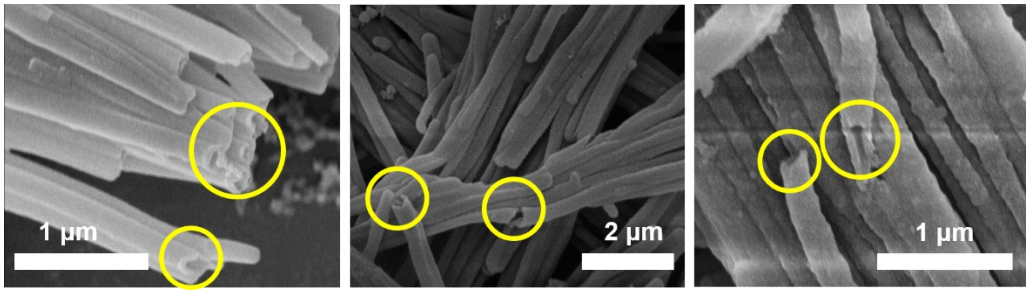

Figure S14. SEM image of **bPDI-AHD-TPH** tubular bundles (yellow circle show the hollow inner structures of the tubes).

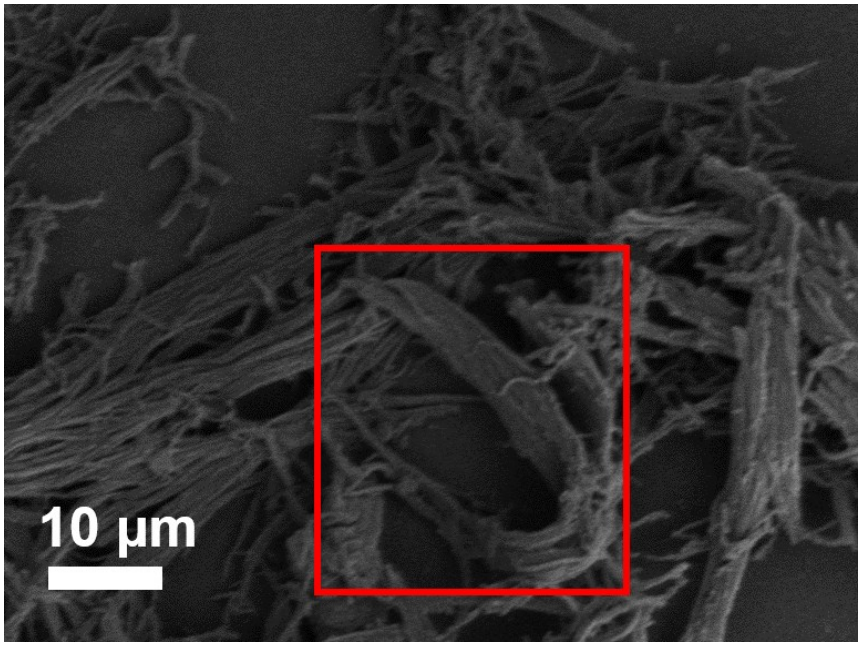

Figure S15. SEM image of **bPDI-AHD-TPH** with bending angle indicating the flexibility of the tubular bundles.

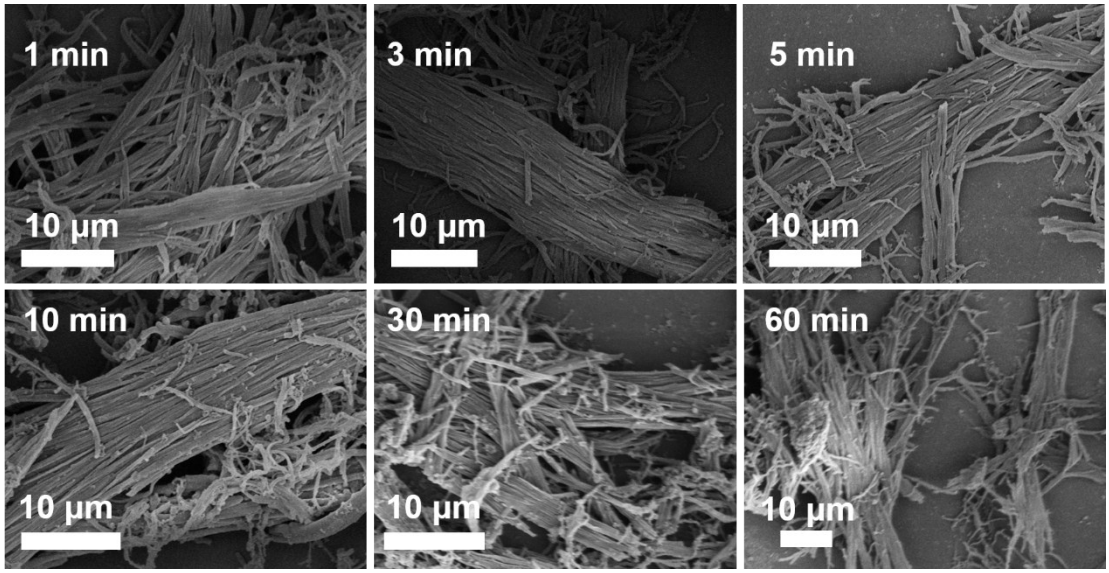

Figure S16. SEM images of **bPDI-AHD-TPH** after ultrasonic treatment for 1, 3, 5, 10, 30 and 60 min, respectively.

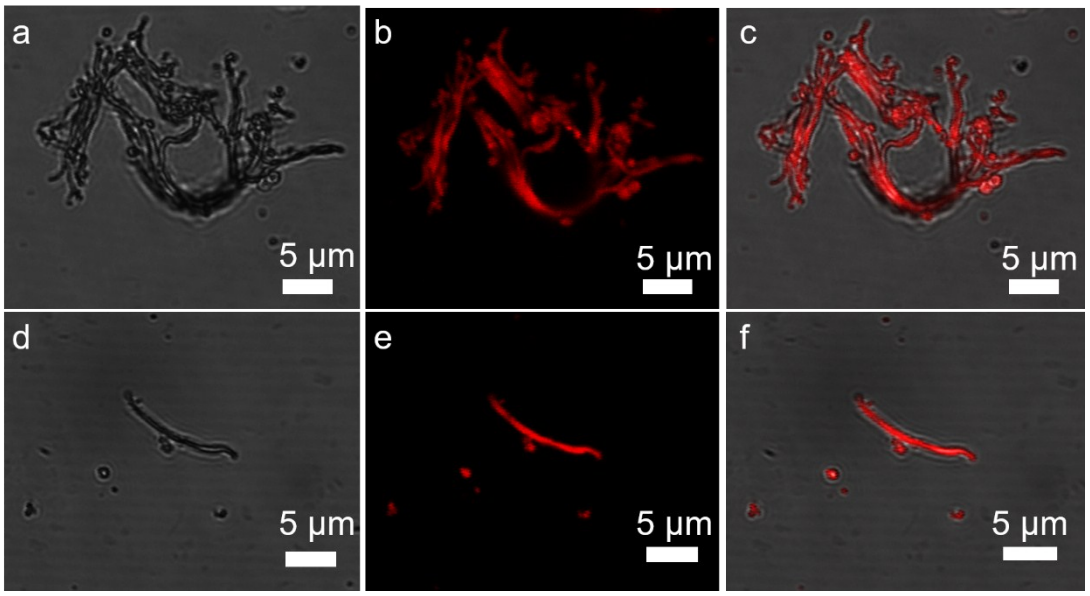

Figure S17. (a, d) Bright-field images. (b, e) CLSM images (c, f) Merged bright-field and CLSM images of **bPDI-AHD-TPH**.

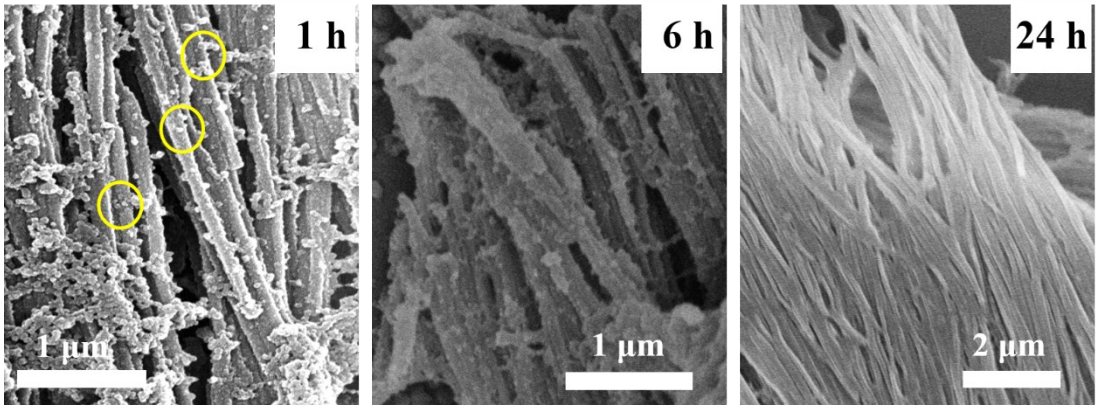

Figure S18. SEM images of **bPDI-AHD-TPH** recorded at different intervals of time.

Table S2. The diameters and lengths of the monomer and polymer at different reaction time.

Sample	Diameter/nm	Length/μm
TPH	65-134	10-30
bPDI-AHD-TPH (1 h)	93-231	10-30
bPDI-AHD-TPH (6 h)	128-347	20-40
bPDI-AHD-TPH (24 h)	166-360	30-60

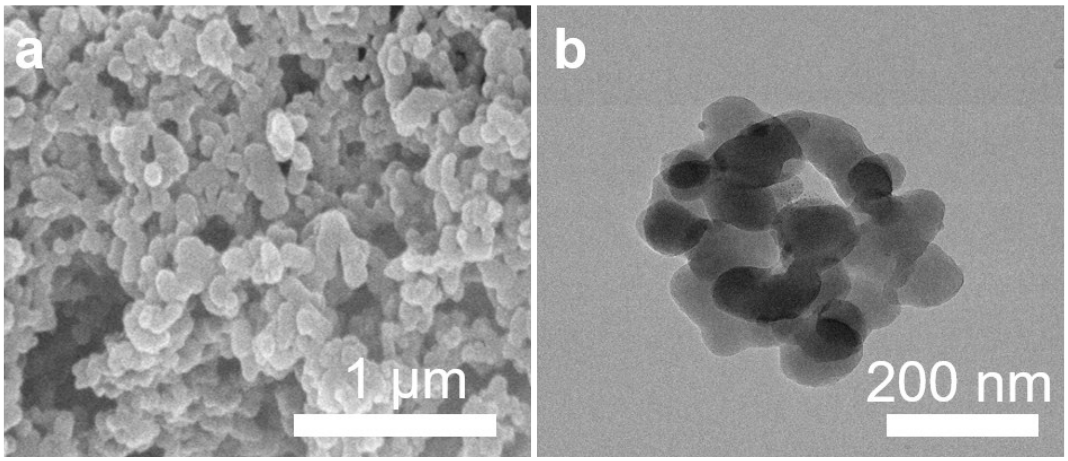

Figure S19. (a) SEM and (b) TEM images of **bPDI-AHD-TPH** obtained under magnetic stirring without changing the other conditions.

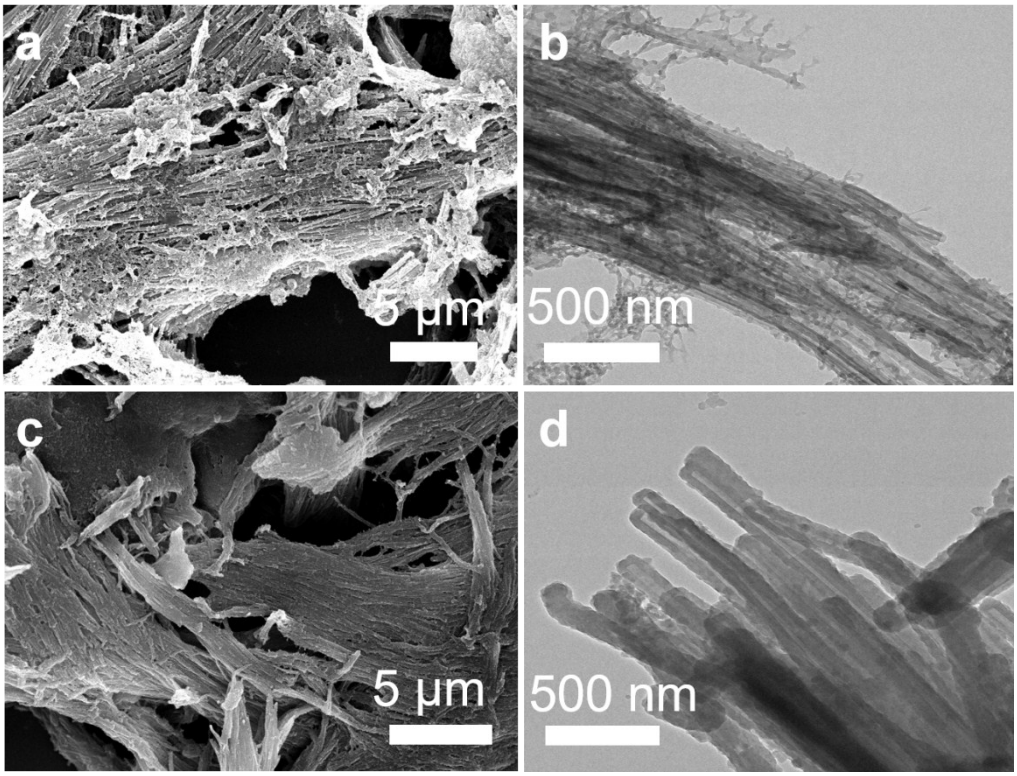

Figure S20. SEM and TEM images of **Ph-AHD-TPH** (a, b) and **BiPh-AHD-TPH** (c, d).

4. Morphology control under different reaction conditions

The reaction conditions including the solvent, substrate concentration, and reaction temperature were screened for the synthesis of **bPDI-AHD-TPH**.

Table S3. Reaction conditions screening for the synthesis of **bPDI-AHD-TPH**.

Entry	Solvents							Temp.	Time
	DMAc	*o*-DCB	DMF	DMSO	NMP	EG	AcOH (6M)		
1	2 mL						0.2mL	120	3 days
2		2					0.2mL	120	3 days
3			2				0.2mL	120	3 days
4				2			0.2mL	120	3 days
5					2		0.2mL	120	3 days
6						2	0.2mL	120	3 days
7	1						0.2mL	120	3 days
8	4						0.2mL	120	3 days
9	6						0.2mL	120	3 days
10	2						0.2mL	r.t.	3 days
11	2						0.2mL	150	3 days

Note: All reactions were carried out using 0.06 mmol of **bPDI** and 0.04 mmol of **TPH**. The unit of temperature was °C. r.t. represented room temperature.

With respect to solvent

As for the solvent, one significant feature is that the polarity and boiling point of the solvents may have a great influence on the morphology of **bPDI-AHD-TPH**. Different solvents including *N,N*-dimethylformamide (DMF), *N,N*-dimethylacetamide (DMAc), dimethyl sulfoxide (DMSO), 1,2-dichlorobenzene (o-DCB), *N*-methyl pyrrolidone (NMP), ethylene glycol (EG) were used for the synthesis of **bPDI-AHD-TPH**.

With respect to monomer concentrations

To examine the influence of the concentrations of the monomer, different concentration of **bPDI** (0.06, 0.03, 0.015 and 0.01 M) were obtained by using different volume of solvent (1, 2, 4 and 6 mL).

With respect to different temperature

The reaction mixture were distributed to several pyrex tubes and individual samples were treated at different temperatures (r.t., 120, 150 °C).

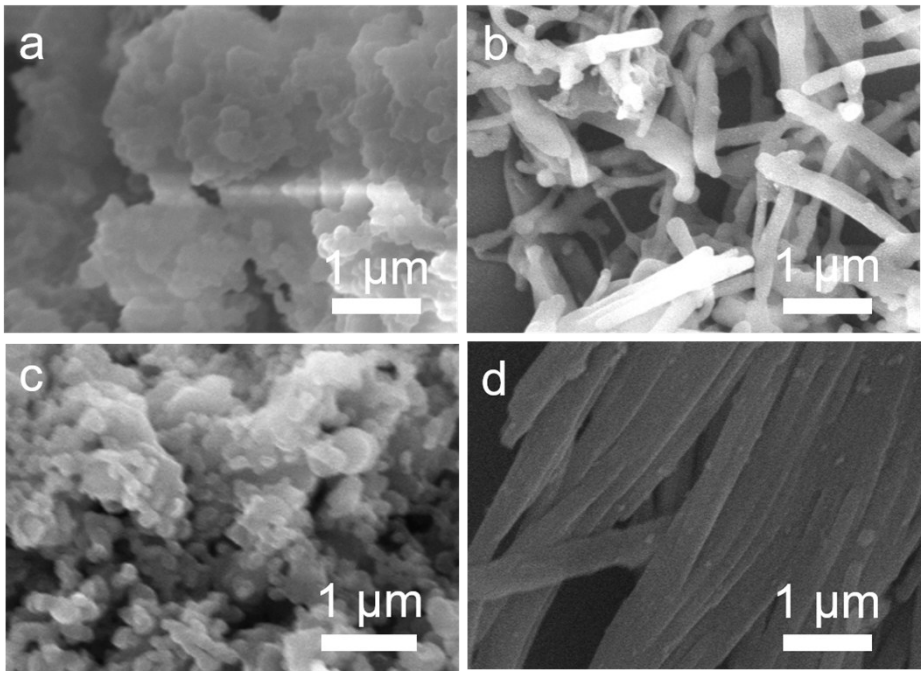

Figure S21. SEM images of **bPDI-AHD-TPH** synthesized in different solvent (a) 1,2-dichlorobenzene, (b) *N,N*-dimethylformamide, (c) *N*-methyl pyrrolidone, (d) *N,N*-dimethylacetamide. (Note: there is no precipitated product observed if using dimethyl sulfoxide or ethylene glycol as reaction solvent)

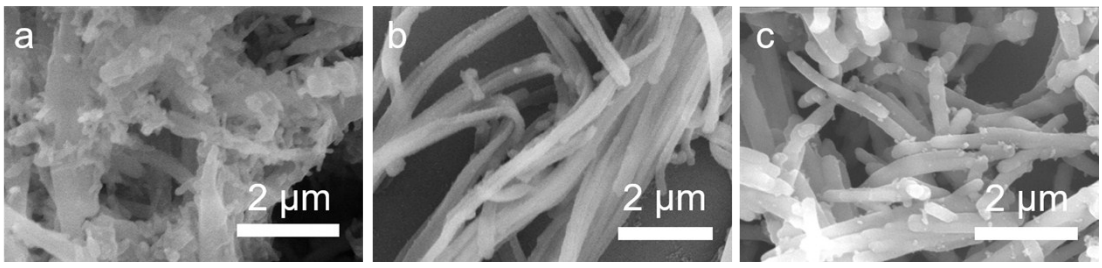

Figure S22. SEM images of **bPDI-AHD-TPH** synthesized at different substrate concentrations. With respect to substrate concentrations of **bPDI**, (a) 0.06 M, (b) 0.03

M, (c) 0.015 M. (Note: there is no precipitated product observed if the concentration of the precursor is 0.01 M).

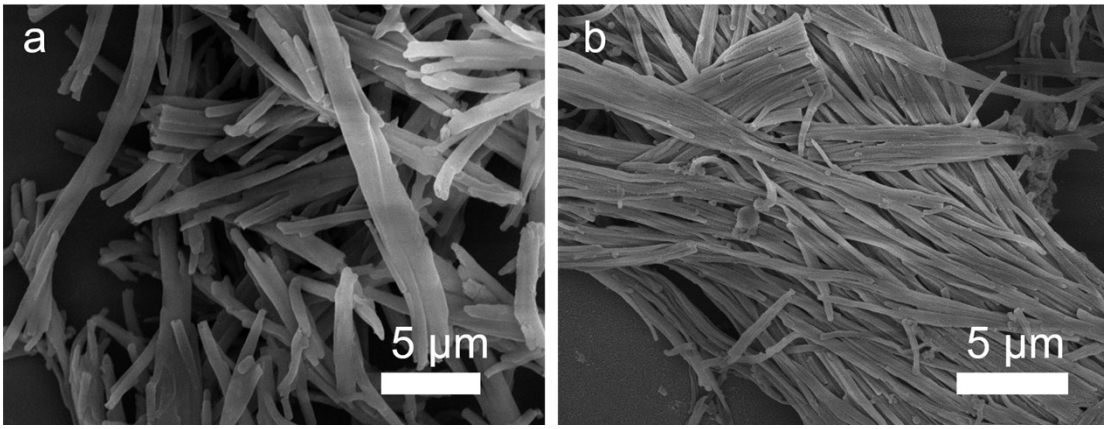

Figure S23. SEM images of **bPDI-AHD-TPH** synthesized at (a) room temperatures and (b) 120 °C. (Note: there is no precipitated product at 150 °C)

5. Figures of bPDI-AHD-TPH film

Figure S24. The equipment for the preparation of the free-standing **bPDI-AHD-TPH** film.

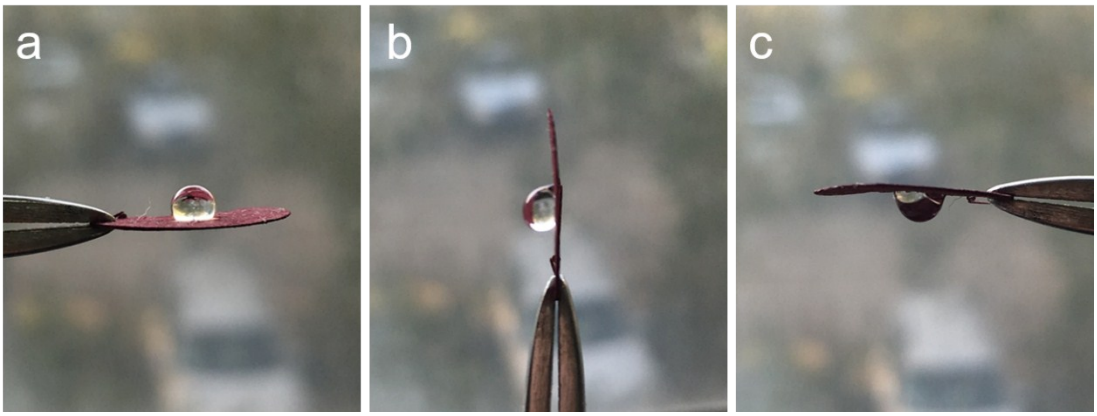

Figure S25. Wettability of **bPDI-AHD-TPH** film. (a) digital picture of water droplet on the film when rotated it 90^{o} (b) and 180^{o} (c).

The **bPDI-AHD-TPH** films show compromised hydrophobicity. The water contact angles for **bPDI-AHD-TPH** is around 136° because of the uniformly distributed heteroatoms, such as oxygen and nitrogen, on the surface. Surprisingly, the spherical droplet can remain pinned to the hydrophobic surface without sliding, even when turned upside-down (Fig. S25), indicating strong adhesion. The droplet remained in the same position without any sliding. This property is vastly required in a wealth of applications, such as biochemical separation, transport of microdroplets *etc*. Therefore, it can be

deduced that cooperation of the hierarchically rough surface and the low surface energy of the **bPDI-AHD-TPH** film leads to sticky hydrophobicity, whereas the widely established methods for sticky hydrophobicity are mainly achieved by creating ordered microscopic arrays on film structures involving sophisticated equipment or time-consuming processes. The strategy developed here has been proved to be a time- and cost-effective method to develop a hydrophobic structure with high adhesion.

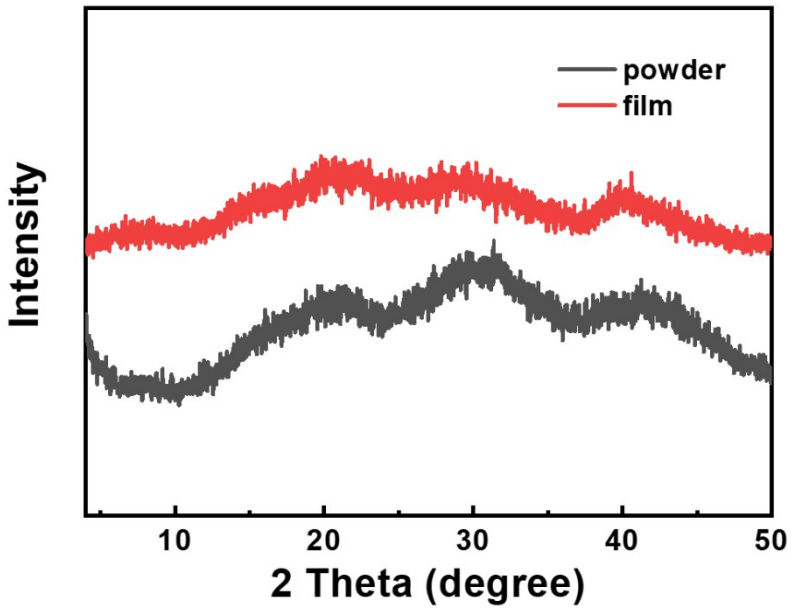

Figure S26. The PXRD patterns of **bPDI-AHD-TPH** in the form of powder and film.

6. Supplementary electrochemical characterization

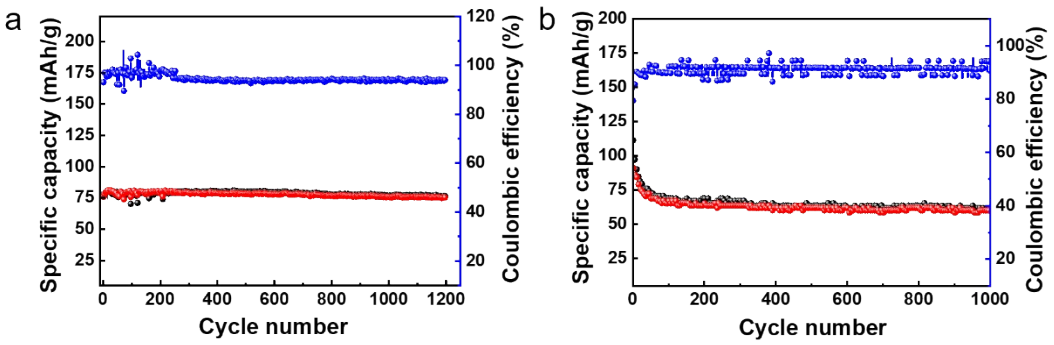

Figure S27. Long-life cycling performance of **bPDI-AHD-TPH** electrode at 3.2 A g^{-1} (a) and at 6.4 A g^{-1} (b) for LIB (discharge-red, charge-black and coulombic efficiency-blue).

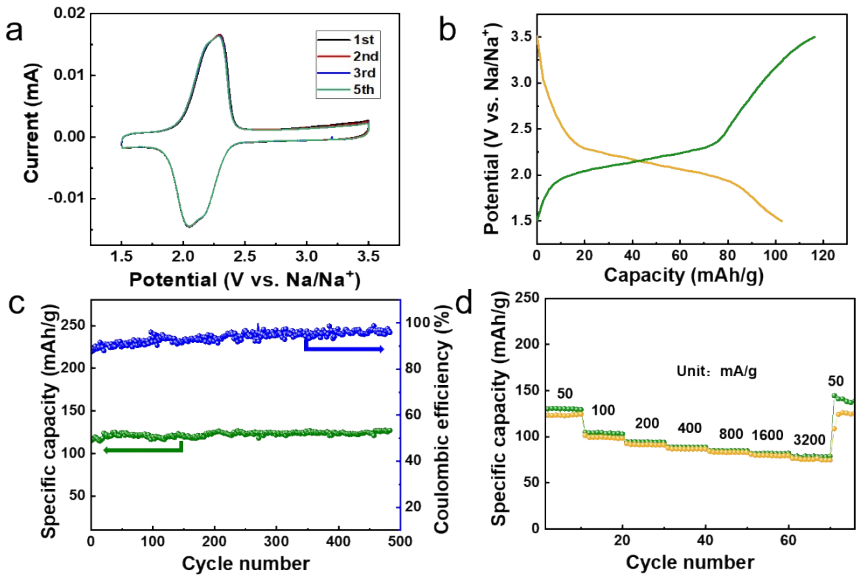

Figure S28. (a) The CV curves of **bPDI-AHD-TPH** at the scan rate of 0.5 mV s^{-1}. (b) Galvanostatic discharge-charge curves of **bPDI-AHD-TPH** electrode at of the current density of 100 mA g^{-1}. (c) Cycling performance of **bPDI-AHD-TPH** electrode at 100 mA g^{-1}. (d) rate capability and coulombic efficiency of **bPDI-AHD-TPH** electrodes upon continuous cycling at different current densities for SIBs.

The electrochemical performances of **bPDI-AHD-TPH** as the sodium ion battery (SIB) cathodes were studied in coin-type cells with Na foil as counter electrode. As shown in Fig. S28, the CV profile of **bPDI-AHD-TPH** at 0.5 mV s^{-1} illustrates two

oxidation peaks at 2.18 and 2.29 V, respectively. Correspondingly, two reduction peaks at 2.17 and 2.06 V can be observed in the reduction scan, assignable to the stepwise insertion and de-insertion of Na^+ ions. In the galvanostatic charge/discharge profiles obtained at 100 mA g^{-1}, the discharge flat platforms appeared at 2.17 and 2.06 V, and two charge flat platforms were found at 2.18 and 2.29 V, confirming a two-stage redox process of **bPDI-AHD-TPH** with Na^+. As shown in Fig. S28, the capacity of **bPDI-AHD-TPH** as the SIBs cathode is about 120 mA h g^{-1} at 100 mA g^{-1}, which shows no decay even after 500 charge-discharge cycles. **bPDI-AHD-TPH** also exhibits excellent rate capabilities by delivering the capacities of 123, 99, 91, 87, 83, 80, 75 and 124 mA h g^{-1} at current densities of 50, 100, 200, 400, 800, 1600, 3200 and 50 mA g^{-1}, respectively.

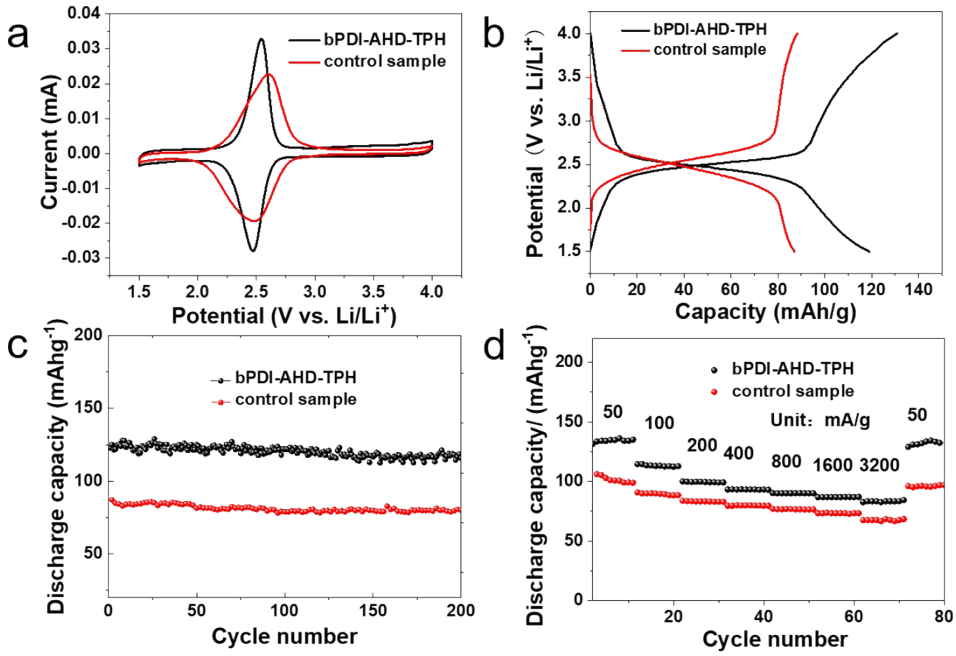

Figure S29. (a) The CV curves of **bPDI-AHD-TPH** and control sample at the scan rate of 0.5 mV s^{-1}. (b) Galvanostatic discharge-charge curves of **bPDI-AHD-TPH** and control sample electrode at the rate of 100 mA g^{-1}. (c) Cycling performance of **bPDI-AHD-TPH** and control sample electrode at 100 mA g^{-1}. (d) rate capability of **bPDI-AHD-TPH** and control sample electrodes upon continuous cycling at different current densities.

The electrochemical performances of **bPDI-AHD-TPH** and the control sample as the cathode materials for lithium ion battery (LIB) were evaluated by fabricating a series of coin-type cells with metallic Li foil as the counter electrode. The cyclic voltammetry (CV) curves of **bPDI-AHD-TPH** and the control sample were first recorded in the voltage range of 1.5 - 4.0 V (vs. Li/Li^+) at the scan rate of 0.5 mV s^{-1}. As shown in Fig. S29, both polymers manifested one well-resolved oxidation peak at 2.54 V (2.62 V for the control sample) and a reduction peak at 2.46 V (2.47 V for the control sample), corresponding to the insertion and de-insertion of Li atoms (Fig. S29). The small gaps (0.08 V) between the reduction and oxidation peaks should be due to the large electrode reaction rates of **bPDI-AHD-TPH**. And the closed hysteresis between the reduction and oxidation peak is supposed to render better cycling stability of **bPDI-AHD-TPH** than the control sample.

As shown in Fig. S29c, **bPDI-AHD-TPH** delivers a high reversible capacity of 122 mA h g^{-1} at the current density of 100 mA g^{-1}, which can be maintained even after 200 cycles. Although the capacity of the control sample in the galvanostatic charge/discharge tests is only ~ 85 mA h g^{-1}. The rate capability of the LIB cathodes based on **bPDI-AHD-TPH** and the control sample are compared in Fig. S29d. The capacities of **bPDI-AHD-TPH** at the current densities of 50, 100, 200, 400, 800, 1600, 3200 and 50 mA $g^{-1}$are 133, 113, 100, 93, 90, 87, 83 and 132 mA h g^{-1}, respectively, which are higher than those of the control sample under the same conditions. Different from the PDI unit of the control sample linked *via* the imide groups, the bay-position substituted **bPDI** can adopt a torsion configuration within the scaffold of the polymer, thus relieving the dense face-to-face stacking of its aromatic framework and enabling the release of its exceptional semiconducting characters, such as high charge carrier mobility and redox activity.

Table S4. The performance comparison of bPDI-AHD-TPH vs. the recently reported organic cathodes materials for LIBs and SIBs.

Sample name	Initial/Final capacity	Capacity retention (Cycle number)	Current density (mA g^{-1})	Reference
3PDMI-Li	126/95	75% (30)	36	J. Am. Chem. Soc. 2017, 139, 6635.[4]
PI-Br-Na	58/78	119 (100)	22	Adv. Energy Mater. 2017, 7, 1701316.[5]
PI@CNT-Li	200/165	82.5% (200)	150	Angew. Chem. Int. Ed. Engl. 2018, 57, 7146.[6]
PI@CNT-Na	160/150	94% (50)	150	Angew. Chem. Int. Ed. Engl. 2018, 57, 7146.[6]
PTCDA/RGO/CNT-Li	96/90	94% (500)	200	Adv. Funct. Mater. 2018, 28, 1804629.[7]
2D-PAI@CNT-Li	104/104	100% (50)	100	Adv. Mater. 2019, 1901478.[8]
PI-PMDA@CNT-Li	81/66	81% (50)	100	Adv. Mater. 2019, 1901478.[8]
bPDI-AHD-TPH-Li	122/117	96% (200)	100	This work
bPDI-AHD-TPH-Na	102/120	118% (500)	100	This work

7. Reference

(1) Rajasingh, P.; Cohen, R.; Shirman, E.; Shimon, L. J.; Rybtchinski, B. Selective Bromination of Perylene Diimides under Mild Conditions. *J. Org. Chem*. **2007**, 72, 5973.

(2) He, C.; Lin, Z.; He, Z.; Duan, C.; Xu, C.; Wang, Z.; Yan, C., Metal-tunable nanocages as artificial chemosensors. *Angew. Chem., Int. Ed*. **2008**, 47, 877.

(3) Ye, Y.; Zhang, L.; Peng, Q.; Wang, G.-E.; Shen, Y., Li, Z.; Wang, L.; Ma, X.; Chen, Q.-H.; Zhang, Z.; Xiang, S. High Anhydrous Proton Conductivity of Imidazole-Loaded Mesoporous Polyimides over a Wide Range from Subzero to Moderate Temperature. *J. Am. Chem. Soc*. **2015**, 137, 913.

(4) Kim, D. J.; Hermann, K. R.; Prokofjevs, A.; Otley, M. T.; Pezzato, C.; Owczarek, M.; Stoddart, J. F. Redox-Active Macrocycles for Organic Rechargeable Batteries. *J. Am. Chem. Soc.* **2017**, 139, 6635.

(5) Banda, H.; Damien, D.; Nagarajan, K.; Raj, A.; Hariharan, M.; Shaijumon, M. M. Twisted Perylene Diimides with Tunable Redox Properties for Organic Sodium-Ion Batteries. *Adv. Energy Mater*. **2017**, 7, 1701316.

(6) Fan, X.; Wang, F.; Ji, X.; Wang, R.; Gao, T.; Hou, S.; Chen, J.; Deng, T.; Li, X.; Chen, L.; Luo, C.; Wang, L.; Wang, C. A Universal Organic Cathode for Ultrafast Lithium and Multivalent Metal Batteries. *Angew. Chem., Int. Ed*. **2018**, 57, 7146.

(7) Zhou, G.; Miao, Y.-E.; Wei, Z.; Mo, L.; Lai, F.; Wu, Y.; Ma, J.; Liu, T. Bioinspired Micro/Nanofluidic Ion Transport Channels for Organic Cathodes in High-Rate and Ultrastable Lithium/Sodium-Ion Batteries. *Adv. Funct. Mater*. **2018**, 28, 1804629.

(8) Wang, G.; Chandrasekhar, N.; Biswal, B. P.; Becker, D.; Paasch, S.; Brunner, E.; Addicoat, M.; Yu, M.; Berger, R.; Feng, X. A Crystalline, 2D Polyarylimide Cathode for Ultrastable and Ultrafast Li Storage. *Adv. Mater*. **2019**, 1901478.